ORIGINAL PAPER

On the accuracy of the SGP4 to predict stellar occultation events using ENVISAT/GOMOS data and recommendations for the ALTIUS mission

Jan Thoemel[1,2] · Nina Mateshvili[2] · Philippe Demoulin[2] · Filip Vanhellemont[2] · Didier Pieroux[2] · Christine Bingen[2] · Emmanuel Dekemper[2] · Ghislain Franssens[2] · Charles Robert[2] · Didier Fussen[2]

Abstract

In preparation for the operations of the ALTIUS mission, research is carried out to assess the accuracy of the SGP4 orbital propagator in predicting stellar occultation events. The quantification of the accuracy and its consequent improvement will enable reliable measurement planning and, therefore, maximize the number of measurements. To this end, predictions are made for the timing of occultations for the GOMOS instrument on-board the ENVISAT, which are then compared to actual occultation occurrences. It is found that the error is substantial but follows a trend that can be interpolated. This enables devising a method for highly accurate predictions given a sufficient number of data points. Statistically significant results for the accuracy of the propagator and a calibration method are presented. Recommendations for a measurement planning procedure of ALTIUS are formulated.

Keywords SGP4 · Astrodynamics · Accuracy · GOMOS · ENVISAT · ALTIUS

1 Introduction

After an exhaustive study phase conducted by the Royal Belgian Institute for Space Aeronomy (BIRA-IASB),[1] the Belgian Science Policy Office (BELSPO) proposed, to the European Space Agency, the implementation of the ALTIUS mission [1] in late 2016. It features a space segment of a PROBA-class satellite [2] with a three-channel imaging spectrometer to conduct limb scatter, solar, lunar, planetary, and stellar occultation observations. The satellite is shown in Fig. 1 and an overview of the observation modes in Fig. 2. The occultation mode is explained in Fig. 3. The limb-viewing capability allows altitude-resolved measurements of the chemical composition of the stratosphere. Further system components are a Flight Operations Segment (FOS) and a Payload Data Ground Segment (PDGS) in charge of the measurement planning and the data processing.

The mission will investigate the chemical dynamics of the middle atmosphere [3]. More importantly, it will take routine and global measurements of the vertical profile of ozone concentration, allowing improving weather forecast and confirmation of the recovery of the ozone layer, which is now anticipated but far not verified. Although the initial measurements appear to do so as illustrated in Fig. 4, future observations are required to rule out natural variability and erroneous conclusions due to noise or other measurement shortcomings.

In addition, recent research [5] revealed an unexpected reduction in decline of ozone depleting substances attributed to illegal production of CFC-11. This requires uninterrupted global and accurate monitoring of the ozone content in the atmosphere, for instance, through the ALTIUS mission.

2 Motivation

Due to the intended routine ozone measurements, ALTIUS is partially driven by operational mission requirements. Therefore, the measurements need to be planned reliably and well in advance to ensure a smooth and long-term delivery of the ozone data within 3 h from the instant of measurement

✉ Jan Thoemel
jan.thoemel@gmail.com

1 GomSpace Sarl, 9 Avenue des Hauts-Fourneaux, 4362 Esch-sur-Alzette, Luxembourg

2 Royal Belgian Institute for Space Aeronomy, Avenue Circulaire 3, 1180 Uccle/brussels, Belgium
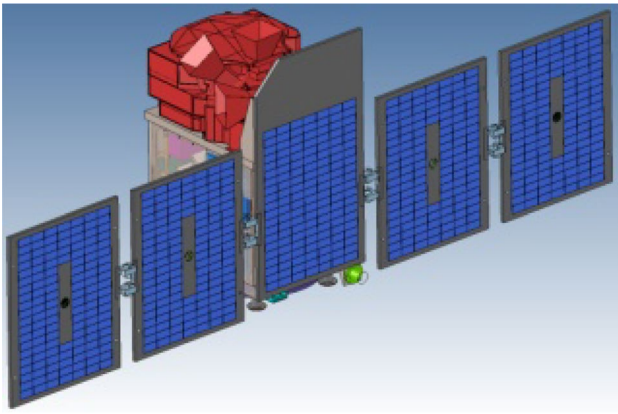
---

1 Affiliation of the authors.

Fig. 1 Preliminary CAD model of the ALTIUS satellite, which is based on the PROBA concept
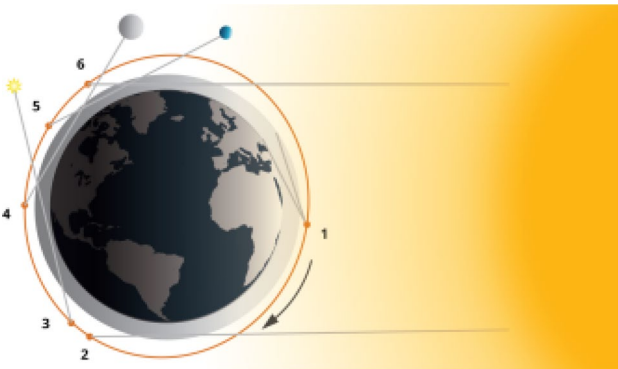

Fig. 2 Different observation modes: 1 limb scatter; 2 solar occultation (set); 3 stellar occultation (rise); 4 lunar occultation (rise); 5 planetary occultation (rise); 6 solar occultation (rise). Not shown are stellar, lunar, and planetary occultations, while celestial body is setting

until reception by the users—called Near Real-Time (NRT) delivery.

The ALTIUS satellite will be in a sun-synchronous orbit (SSO), with the main characteristics as listed in Table 1, from which it will take, per orbit, up to 100 bright limb measurements on the sun-lit side of the earth. It will also take two solar (rise and set) occultations measurements at dawn and dusk, and up to 10 stellar/planetary occultation measurements at the night side. In addition, ALTIUS may carry out lunar occultation measurements.

The bright limb measurements are not particularly challenging from an operational planning point of view as they only require orienting the spacecraft towards the sun-lit atmospheric horizon. The exact position of the measurement location, as well as the satellite position and attitude need to be known a posteriori.

In contrast to the relatively simple needs of bright limb measurements, stellar occultation measurements require a

precise prediction not only in terms of line-of-sight direction, as the target is small, but also in terms of timing. As the pass of a star behind the atmosphere lasts only on the order of minutes from a low earth orbit, the satellite needs to point at the star at the right time. To avoid unnecessary waiting time, the occultation event needs to be accurately predicted. Excessive waiting time reduces the number of achievable occultation measurements per orbit.

In the past, several investigations have been made into the accuracy of the Simplified General Perturbations Satellite Orbit Model 4 (SGP4) [6] in terms of position accuracy, e.g., longitude, latitude, and altitude [7–10][2]. However, here, knowing the position accuracy is not sufficient, because it does not allow concluding on the accuracy to predict occultation timing. Investigations into the occultation timing accuracy are largely missing, which might be explained to some extent by the fact that stellar occultations were and are not measured routinely. The ALTIUS mission requires such an assessment to plan its measurement campaign. It is expected that measurement planning will be needed around 1 or 2 months ahead for a duration of about 1 month, which is much longer than the planning durations for ENVISAT/GOMOS, but considers the high-reliability operational character of the mission.

The capability of propagators, among them the SGP4, to predict an occultation event accurately is an objective of BIRA-IASB's recent research. To this end, past occultation measurements of the Global Ozone Monitoring by Occultation of Stars (GOMOS) instrument on-board the ENVIronmental SATellite (ENVISAT) are predicted using the SGP4 and related Two Line Elements (TLEs) as the initial condition. The predictions are then validated against actual occultation event occurrences. A notable difference between ENVISAT/GOMOS and ALTIUS is that the former carried out only star setting occultation measurements, whereas the latter will also take measurements during star rises. The investigation into the accuracy of the SGP is carried out here for durations much longer than strictly needed for ALTIUS. This will enable greater insight and thorough conclusions. In addition, as the method will be validated against data obtained with ENVISAT, its validity will be limited to orbits similar to those of ENVISAT[3] and maneuvers of similar magnitude.

---

[2] The SGP4 together with its related data set—the Two Line Elements (TLE)—is widely used and is thus a *de-facto* standard method for trajectory modeling, as it is well documented and implemented in many applications. An alternative is, for instance, the CCSDS ODM, which is also widely used by space agencies. However data sets are not easily available.

[3] See also Fortescue et al. [11] and Aida et al. [10] for a qualitative and quantitative overview of all perturbations to objects in orbit around the Earth.

Fig. 3 Illustration of the occultation technique. While the satellite advances on its orbit, the line of sight passes through lower and lower atmospheric layers. The lower the apparent tangent point, the higher is the diffraction, i.e., the bending of the light rays. It is negligible at higher layers above around 60 km
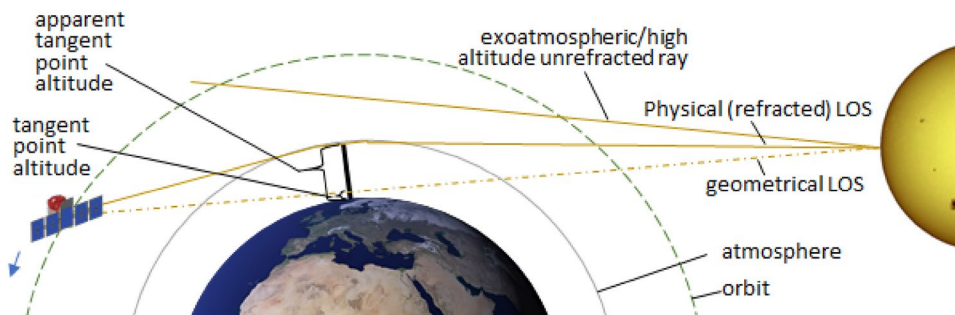
Fig. 4 Trend of atmospheric ozone: data assembly from different satellite measurements and parabolic trendline; reproduced from [4]
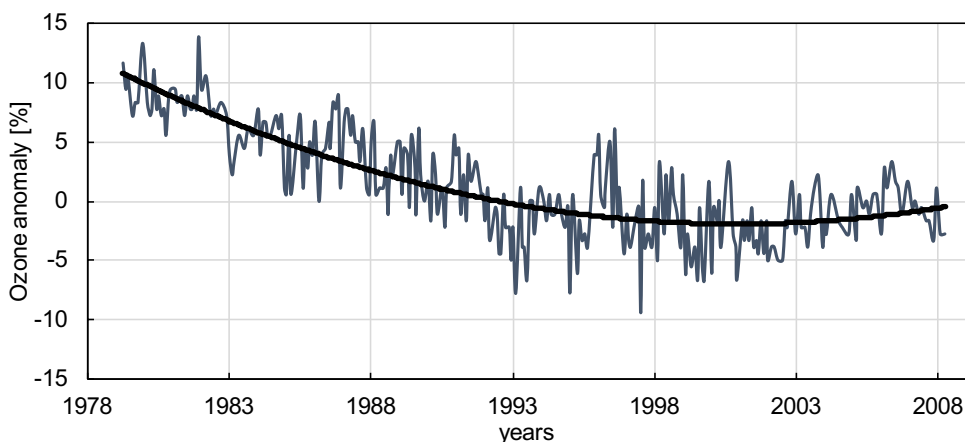
Table 1 Main orbital characteristics of the ALTIUS mission [1]

Altitude	Type	Ground track revisit time
680 km	SSO 10:00–14:00	3 days, i.e., 800-km distance of consecutive ground tracks at the equator

With understanding of the accuracy of the occultation prediction, a method may be devised to correct inaccurate predictions. This method is called calibration here. Ideally, such a method is robust, i.e., can address several or all sources of uncertainty and reduce it, and is simple. If the method is computationally efficient enough, it may be implemented in the on-board software enabling part of the mission planning to be conducted by the space craft itself without delayed ground intervention.

In the following Sect. 3, the conventional method for predicting the trajectory is presented as well as occultation events. Moreover, data for the trajectory and occultation events, obtained through measurements, and which used for validation of the methods are summarized. In addition, factors that influence the accuracy, i.e., space weather effects, are elaborated on. Then, we proceed to explain our method to improve the prediction of occultation events. The results are discussed in Sect. 4. In Sect. 5, recommendations for the planning of the measurement campaign for the ALTIUS mission are formulated. Conclusions are drawn in Sect. 6.

3 Computational methods and validation data

The investigation into the accuracy of orbital predictors is carried out for the SGP4. To begin with, it is validated against two data sets verifying the altitude and the semi-major axis accuracy. Such data are obtained from publicly available TLEs and the Doppler Orbitography and Radio-positioning Integrated by Satellite (DORIS) instrument on-board the ENVISAT (Fig. 5). Afterwards, the prediction accuracy for occultation events is verified with data from the GOMOS instrument also on-board the ENVISAT. The locations of both instruments are shown in Fig. 6.

3.1 Orbit modeling and occultation timing prediction

An implementation of the SGP4 in Systems Tool Kit (STK) version 11.2 by Analytics Graphics, Inc. (AGI) has been used to predict loss of line of sight (LOS) between the ENVISAT spacecraft and selected stars at star set during the

Fig. 5 ENVISAT in orbit with deployed appendices (artistic, credit: ESA)

Fig. 6 ENVISAT with stowed solar panel and radar instrument. Highlighted are the two instruments from which data are used for this study (credit: ESA)

period of April 2011 until the failure of the satellite approximately 1 year later, in April 2012.

In total, 13 trajectories have been propagated from different starting instants: every 4 weeks, commencing 27 April 2011 (Wednesday). For each, a TLE was used to predict the orbit of the satellite and the loss of LOS from the TLE's epoch. TLEs have been obtained from the Celestrak[4] website and are listed in Table 6 (Appendix B).

The stars selected for this investigation, together with their main characteristics and the number of occultations measured, are listed in Table 5 (Appendix A). The number

Table 2 Statistical data: number of occultation events and their dispersion per period

	Number of occultations for calibration (-)	Occultation time standard deviation (d)
Period 1	0	–
Period 2	54	3.3166
Period 3	401	6.7823
Period 4	380	7.9373
Period 5	342	7.6485
Period 6	159	7.9373
Period 7	133	5.9161
Period 8	48	5.0498
Period 9	0	–
Period 10	15	0.70711
Period 11	12	1.5811
Period 12	48	4.4721
Period 13	50	7.3598
Period 14	57	2.7386
Period 15	0	–

of occultations and the occultation time standard deviation are shown per period in Table 2. Latter is a measure of how close the occultation event is clustered together. The higher the value, the more spread they are within a period; see also Fig. 10.

3.2 Two line elements

The accuracy of the trajectory prediction is first validated in terms of the semi-major axis. To this end, an exhaustive set of additional TLEs is obtained from Celestrak. Up to two data sets per day are used over the investigation period. The TLEs yield the mean motion n, which is used to compute the orbital period:

$$T = \frac{2\pi}{n}. \tag{1}$$

The semi-major axis is computed through:

$$a = \sqrt[3]{\frac{\mu T^2}{4\pi^2}}, \tag{2}$$

where $\propto$ is the standard gravitational parameter for Earth. The formulas used here are strictly speaking valid only for Keplerian orbits, whereas the TLEs, however, constitute Brouwer–Lyddane elements [12]. Therefore, the computed values are only indicative but considered sufficiently accurate to support the conclusion of this research.

---

[4] https://www.celestrak.com/.

Fig. 7 Comparison of semi-major axes: (1) based on TLEs, i.e., measured through ground-based facilities; (2) computed, with SGP4/STK (4 of 13) using TLE as the initial condition, with linear trend lines, and derivative of mean motion (right axis)
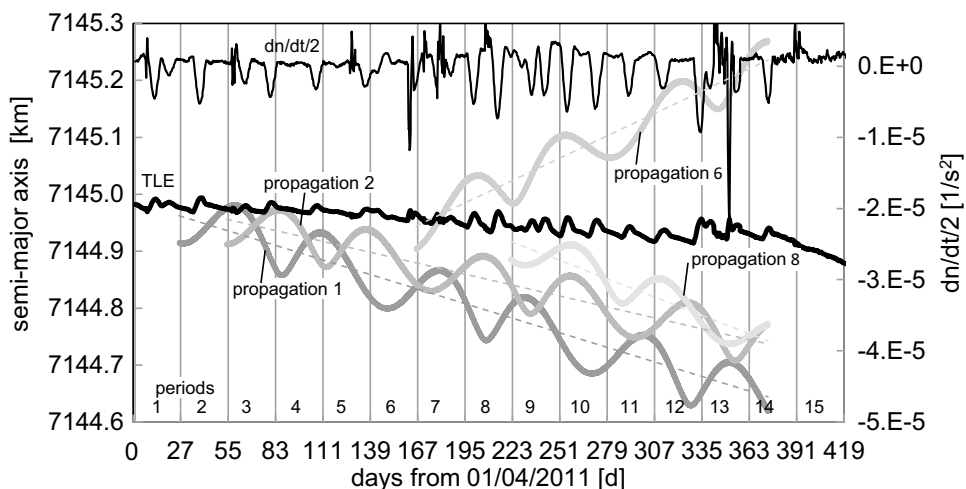
Figure 7 shows the TLE-derived semi-major axis over the investigation period, which is divided into 15 periods. The derivative of the mean motion, also shown, is an indicator of the rate of change of the semi-major axis (and altitude). It can be seen that the semi-major axis is subject to decay and regular increases until before the failure of the satellite on the 8th April 2012 (day 374 in period 14). The first is attributed to the atmospheric drag and the latter are due to orbital raise maneuvers of the satellite. The derivate of the mean motion is consistent with this observation.

In Fig. 7, the semi-major axis predictions of 4 out of the 13 propagations[5] of the SGP4 are shown. They show either a declining or a rising characteristics depending on the initial TLE set used. The semi-major axis is rising if an initial condition TLE is obtained during an orbit raise maneuver.

3.3 ENVISAT DORIS data

As additional validation of the SGP4 predictive capabilities, the highly accurate orbit measurements of ENVISAT's DORIS experiment [13] are being used. Data are obtained from ESA's Earth observation portal.[6] The experiment provides the state vector once per minute, from which the apogee and perigee are inferred here, and consequently, the semi-major axis is determined. The latter is compared with the TLE obtained semi-major axis in Fig. 8.

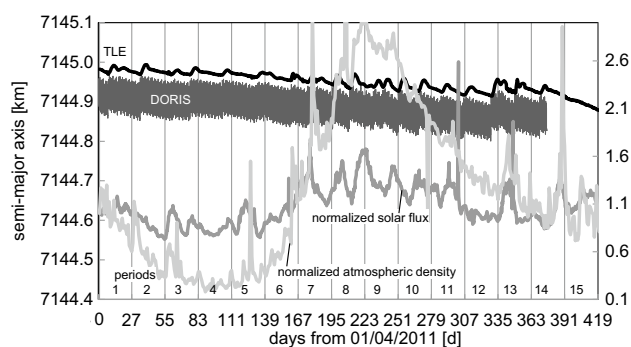The characteristics of the observed ENVISAT trajectory for the investigation period are summarized in Table 3.

Fig. 8 Solar activity, atmospheric density (right axis), and ENVISAT's semi-major axis as obtained by TLEs and by the DORIS instrument (left axis) during the investigation period

Table 3 ENVISAT's relevant orbit characteristics during investigation period

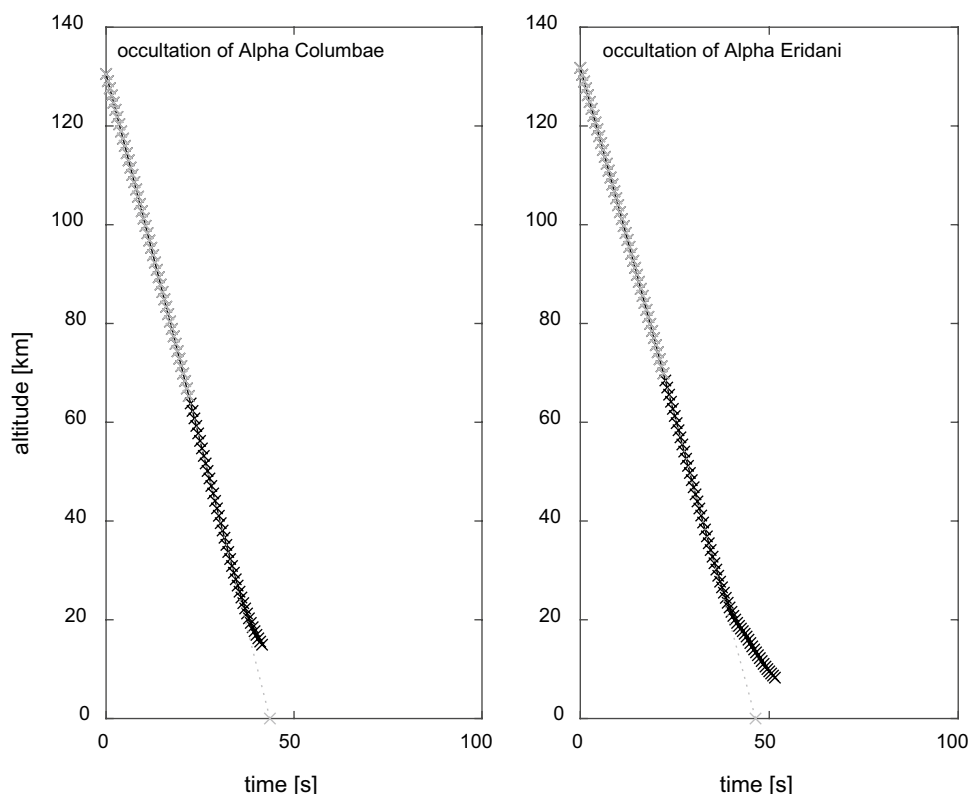| Orbit characteristic	Value (TLE)	Value (DORIS)
Maximum semi-major axis (km)	7144.9936	7145.0117
Minimum semi-major axis (km)	7144.7567	7144.7862
Mean semi-major axis (km)	7144.9193	7144.8869
Standard deviation semi-major axis (km)	0.0604	0.0426
Number of orbit raising maneuvers (-)	~23	

3.4 Assessment of space weather influence

The solar activity influences the atmosphere and can be characterized by the 10.7 cm radio flux. Data of this radio flux, which is a proxy for atmosphere-heating solar activity, can be obtained through public Internet services such

---

[5] Not all 13 are shown for clarity of the viewgraph.

[6] https://earth.esa.int/.

Fig. 9 Examples of the evolution of the ATP altitude over time with its extrapolation to zero altitude. Only the gray points are being used to extrapolate to zero altitude to avoid falsification caused by refraction effects

as the Canadian space weather website.[7] Atmospheric heating tends to expand the atmosphere and, therefore, increase the atmospheric density and, consequently, satellite drag. The variability of the density and, therefore, drag as a consequence to solar radiation is most relevant below 600-km altitude but not negligible at the altitudes of ENVISAT and ALTIUS in question here.

In addition, the atmospheric density can be directly obtained from an NASA-maintained website providing the MSISE90 atmospheric model.[8] The atmospheric neutral density at an altitude of 800 km at 45° longitude and 55° latitude is used as a representation.

The solar flux and the atmospheric density, normalized by their values at the beginning of the investigation period, are shown, together with the semi-major axis of ENVISAT as derived from TLEs and the DORIS instrument in Fig. 8. The investigation period falls into the ascending phase of solar cycle 24. An initial decrease, and later an increase and further decrease of the sun's activity, with a minimum of about 0.7 and a maximum of 1.5, can be observed. This variability is reflected in the atmospheric density during the period that changes drastically. Initially, it is relatively low, and by the middle of the period, it reaches approximately 20 times its lowest value. The higher density and drag would

require stronger or more numerous orbit raise maneuvers to maintain the altitude of the satellite, the latter of which is visible in the TLE-derived semi-major axis and the derivative of the mean motion data (Fig. 7, periods 8–10).

3.5 GOMOS occultation data

The data of occultation measurements of GOMOS are also available through the ESA EO portal. They include, among other things, the evolution of the time and the apparent tangent point (ATP) altitude of each measurement point during an occultation. At altitudes above 60 km, the ATP altitude coincides with the (geometric) tangent point altitude, cf. Figure 4. Such points can be approximated with a linear curve fit. The approximation is used to determine the time instant of the vanishing tangent point altitude. Approximation and extrapolation are illustrated in Fig. 9. This actual loss of geometric LOS can be compared to the loss of LOS as computed by the SGP4. Lower altitude measurement data were neglected due to refraction effects, which are not modeled in our SGP4 computations. This prevents the determination of the loss of physical (refracted) LOS.
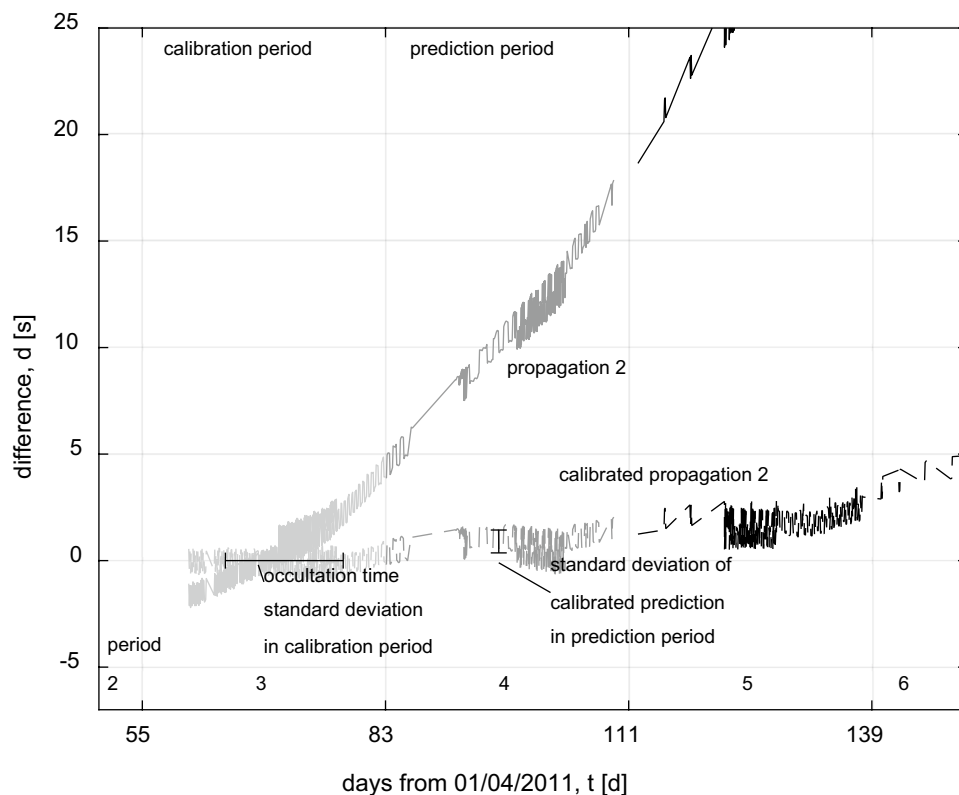
3.6 Calibration and improved predictions

Naturally, the predicted times of loss of LOS deviate from the actual ones, measured by GOMOS. The difference

---

[7] http://www.spaceweather.ca/solarflux/sx-5-en.php.

[8] https://cohoweb.gsfc.nasa.gov/vitmo/msis_vitmo.html.

Fig. 10 Detail of the propagation 2 and calibrated propagation 2 within period 3 (calibration period), 4 (prediction period), and 5

appears to follow approximately a parabola over at least three periods—12 weeks as exemplified for propagation 2 in Fig. 10 (solid line).

This parabolic trend enables to devise a method to predict the difference, i.e., the error. To this end, the error is fit to a polynomial of second order using supporting nodes, i.e., the occultations, in the 4-week period after the propagation start. This period is defined here as the calibration period. The fitted polynomial is then subtracted from the initially predicted timing for the following period, herein called the prediction period, yielding the calibrated propagation:

$$d_{\text{calibrated}} = d_{\text{original}} - (a_1 t^2 + a_2 t + a_3).$$

The calibrated propagation–computation for propagation 2 is also shown in Fig. 10 as dashed line. The error of this calibrated propagation is small and can be measured by its standard deviation in the prediction period.

More data points, i.e., occultations, and higher spread among them, i.e., higher occultation time standard deviation during the calibration period (cf. to Sect. 3.1), will yield a better polynomial fit with smaller error in the prediction period.

The method is applied here for all 13 propagations, where possible, i.e., data are available, providing a large data set to test this method.

4 Results

The results of this accuracy investigation are first provided for the semi-major axis and then for the timing of the occultations.

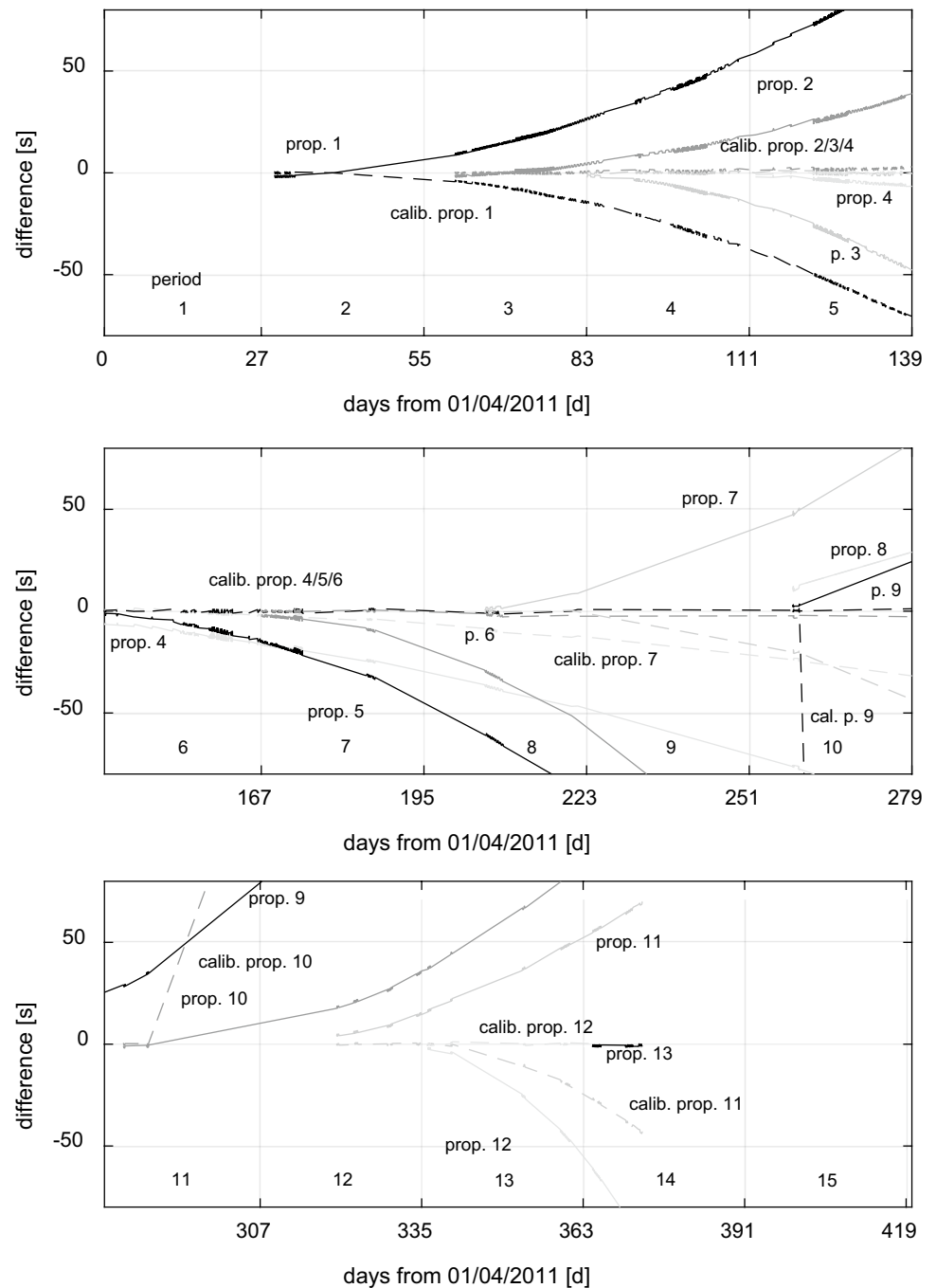### 4.1 Validation of semi-major axis prediction

Figures 7 and 8 show the semi-major axis derived from TLEs and DORIS measurements. The former figure also provides the semi-major axis as simulated by the SGP4 for 4 of the 13 propagations. Several observations can be made.

It can be seen that all data, from the different computational and measurement origins, fall within 700 m (0.01% of total value) over the 60-week-long investigation period.

The means of the semi-major axes of the 13 simulated propagations (shown in Fig. 7, but only 4 of 13) deviate from those of the measured semi-major axes. This is mainly caused by the derivate of the mean motion at the beginning of the simulation imposing a change in altitude. This is, in turn, caused either by drag (altitude decreases) or by an orbit raise maneuver.

The predicted semi-major axes of the simulated propagations show a periodic behavior with duration of around 60 days. This periodicity is considered an artefact of the SGP4 method; it is not a physical phenomenon as it does not appear consistently, i.e., with the same phase, for all

Fig. 11 Timing difference
and corrected timing for each
propagation

propagations. The implementation of the SGP4 into STK has been verified to be correct. The means are considered accurate representations of the simulated propagations.

The actual satellite's altitude is kept approximately constant within 0.1 km[9] by orbit maintenance operations using

the satellite's on-board propulsion system as can be seen in the TLE and DORIS data.

4.2 Validation of timing accuracy

The error, or difference, between the predicted and the measured time of loss of LOS is shown as solid lines for each of the 13 propagations in Fig. 11. In addition, the calibrated difference in timing is shown in the figure as dashed lines, where possible.

Table 4 Statistical data for the occultation event prediction

	Maximum difference (s)	Minimum difference (s)	Mean difference (s)	Standard deviation (s)	Remarks
Calibrated propagation 1	15	3.4	9.1	2.9	
Calibrated propagation 2	2	0.0016	0.9	0.54	
Calibrated propagation 3	1.6	0.00028	0.63	0.48	
Calibrated propagation 4	2.7	0.00016	0.99	0.68	
Calibrated propagation 5	1.5	0.0061	0.6	0.4	
Calibrated propagation 6	3	1.1	2.1	0.55	
Calibrated propagation 7	–	–	–	–	No data are available for period 9 as GOMOS did not carry out any occultation measurement.
Calibrated propagation 8	–	–	–	–	Therefore No predictions can be made by propagation 7 (for period 9) No calibration can be made for propagation 8 (in period 9 and no prediction for period 10)
Calibrated propagation 9	3300	2400	2900	440	
Calibrated propagation 10	510	250	380	92	
Calibrated propagation 11	21	0.039	12	8.1	
Calibrated propagation 12	1.7	0.076	0.79	0.51	
Calibrated propagation 13	–	–	–	–	No prediction is made by propagation 13 as the prediction period falls outside the investigation period (and no data are available due to ENVISAT failure)

It can be seen that all propagations predict an increase in error over time, which is of the order of magnitude of 1 s per day. The error can be positive or negative, depending on whether the derivative of the mean motion—the change in altitude—was positive or negative in the initial TLE set that was used for the propagation.

The propagations that were calibrated yield much smaller error, which can be as little as a few seconds over many weeks. However, the calibration fails for some periods if no or only a few poorly spaced data points have been used,[10] i.e., there is a sparse dispersion of days with occultations within a period. This latter case can be quantified by the occultation time standard deviation, as shown in Table 2.

Statistics of the error in calibrated predicted timing are summarized in Table 4 for those propagations where data are available for calibration and prediction. The accuracy of the prediction is related to standard deviation of the occultation data, as shown in Fig. 12.

One can see that the standard deviation of occultation time within a period, i.e., the spread of the data used for the calibration within the calibration period has a significant impact on the prediction accuracy. The higher the first, the lower, in general, the latter as it would be expected. The prediction accuracy levels off at around 0.64 s if the standard deviation of the occultation time is above 5.9 days.

Further, the maximum error of the calibrated prediction is also shown in Fig. 12. Similar to the predicted occultation time standard deviation, the maximum error decreases substantially with increasing occultation time standard deviation and remains below 3.1 s for an occultation time standard deviation above 5.9 days.

5 Recommended practice for scientific measurement planning for ALTIUS

The assessment of the accuracy of the SGP4, as laid out above, shows that occultation events can precisely and robustly be predicted given approximate initial orbital characteristics and sufficient number of occultation measurements for which apparent tangent point altitude and time are known. Such data are used to calibrate the orbit predictions.
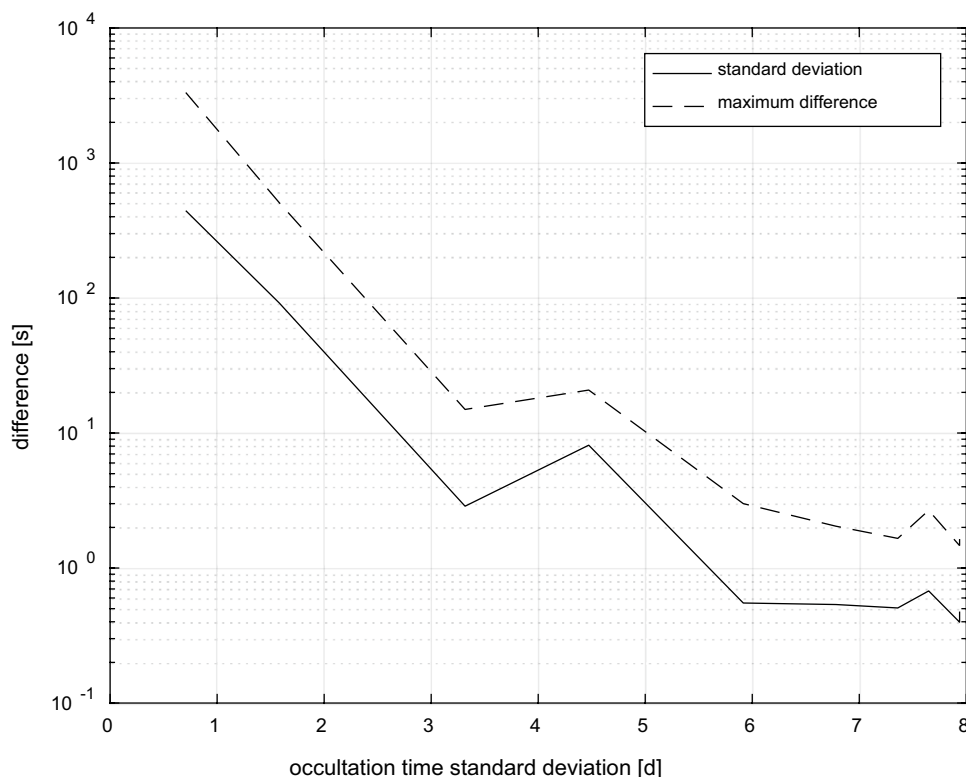
The assessment enables formulating recommendations and devising a procedure to plan the occultation measurements of the ALTIUS mission.

An occultation prediction method may be devised as follows:

1. Eight weeks ahead of the intended scientific measurements:

---

[10] Except for period 9, further data are available on ESA's EO portal that would enable improved predictions. Though the remaining statistical data are considered exhaustive enough to support the conclusions of this research, the poor predictions are kept here to highlight the consequences of poor data for those.

Fig. 12 Prediction difference (standard deviation and maximum difference) versus occultation standard deviation

(a) Obtain a set of TLEs from Celestrak, or another source (provided that the accuracy of the TLEs from the other source is not worse than those of Celestrak).

(b) Propagate the TLEs through the calibration and prediction period, i.e., 4 + 4 weeks, and preliminarily predict the timing of stellar occultations.

(i)Issue measurement plan, i.e., select suitable stellar occultations for the prediction period (weeks 5–8). (Foresee the waiting times for occultation events, either: (i) safe operations: 3.1 s; or (ii) optimized operations: 0.64 s).

2. Four weeks ahead of scientific measurements:

(a) Obtain timing of occultation events during last period, i.e., calibration and period.

(b) Ensure sufficient quality of occultation events, i.e., distribution standard deviation shall be at least 10 days.

(c) Ensure that the orbit maintenance strategy is identical in the calibration and prediction phase.

(d) Compute difference, i.e.. the error, between the initial propagation and a fit of occultation events timing of a second-order polynomial.

(e) Obtain a calibrated timing of the occultations selected for measurement plan by subtracting the error polynomial.

3. At scientific measurement:
   (a) Execute calibrated measurement plan.
4. After execution of measurements:

(a) Verify number of achieved occultations and investigate reasons for failed measurements.

(b) Obtain data related to space weather, i.e., solar flux and atmospheric density, and verify space whether data were of similar behavior in both calibration and prediction phases.

The method can be implemented in the ground or space segment. The latter would provide satellite autonomy at the cost of reduced control by the ground satellite controller. Furthermore, a hybrid approach is also possible: steps 1.(a) until 2.(c) can be carried out on ground and all consequent steps by the satellite.

6 Conclusions

An assessment into the accuracy of the predictions of SGP4 model has been presented. It was carried out by predicting the occurrence of the loss of line of sight during stellar occultation for the GOMOS instrument on-board ENVISAT and comparing it to the actual, measured loss of LOS. The prediction error increases substantially with time. It is possible to fit the error with a parabola and, therefore, calibrate the prediction. The calibrated prediction is substantially better, if enough data of sufficient quality are used.

From the data, one can conclude that occultation events can be predicted with an accuracy of better than 3.1 s and on average with 2.1 s, with a maximum standard deviation of 0.64 s. Because these values can be decreased further if more and better data are used, these constitute highly conservative upper values.

It is remarkable that both factors that highly influence the prediction accuracy—satellite drag and maneuvers[11]—can be accounted for with this simple method.

One may consider the SGP4 an imperfect propagation method and sets of TLEs imperfect initial conditions. However, it is the conviction of the authors that the proposed method consisting of a propagation and calibration would work similarly for other propagation methods and initial condition formats.

These findings enabled to formulate some recommendations that benefit the measurement planning of the ALTIUS mission.

Appendix A

See Table 5.

Table 5 Selected stars for the validation of the occultation event prediction and further key information

Name of star	Hipparcos catalogue number	Right ascension	Declination	Number of occultations
Alpha Phoenicis	2081	00h 26m 17.05 s	−42°18′21.55″	973
Alpha Eridani (Achernar)	7588	01h 37m 42.85 s	−57°14′12.31″	90
Beta Eridani (Cursa)	23875	05h 07m 50.99 s	−05°05′11.21″	3
Alpha Columbae	26634	05h 39m 38.94 s	−34°04′26.80″	129
Alpha Leonis (Regulus)	49669	10h 08m 22.31 s	+11°58′01.95″	1
Gamma Leonis	50583	10h 19m 58.60 s	+19°50′26.00″	1
Gamma Centauri	61932	12h 41m 31.04 s	−48°57′35.54″	12
Delta Centauri	59196	12h 08m 21.54 s	−50°43′20.70″	9
Epsilon Centauri	66657	13h 39m 53.27 s	−53°27′58.90″	38
Iota Centauri	65109	13h 20m 36.07 s	−36°42′43.50″	14
Zeta Centauri	68002	13h 55m 32.43 s	−47°17′17.80″	45
Beta Centauri	68702	14h 03m 49.40 s	−60°22′22.93″	57
Gamma Gruis	108085	21h 53m 55.73 s	−37°21′53.48″	367

The number of occultations per period within the investigation phase is shown in Table 3

---

[11] The method was proven to be valid for orbital raise maneuvers of a magnitude of around 50 m as executed for ENVISAT.

Appendix B

See Table 6.

Table 6 Two line elements used for the propagation of the ENVISAT trajectory

ENVISAT11_17							
1	27386U	02009A	11117.17	9.9E−07	00000–0	47739-4	0
2	27,386	98.5083	185.7912	1216	89.0787	271.055	14.37479
ENVISAT11_21							
1	27386U	02009A	11145.08	5.9E−07	00000–0	34251-4	0
2	27,386	98.5065	213.4164	1108	83.8654	276.2677	14.3748
ENVISAT11_25							
1	27386U	02009A	11173.13	−2.2E−06	00000–0	−57,377	0
2	27,386	98.5055	241.174	965	92.7513	267.3828	14.37477
ENVISAT11_29							
1	27386U	02009A	11201.05	−5.9E−07	00000–0	−50,378	0
2	27,386	98.5042	268.7887	1210	96.8192	263.3134	14.37479
ENVISAT11_33							
1	27386U	02009A	11229.17	−1.9E−06	00000–0	−48,109	0
2	27,386	98.5017	296.6006	1250	90.3983	269.7379	14.3748
ENVISAT11_37							
1	27386U	02009A	11257.15	−2.5E−06	00000–0	−69,470	0
2	27,386	98.4984	324.2639	1102	84.6654	275.4705	14.37482
ENVISAT11_41							
1	27386U	02009A	11285.13	1.53E−06	00000–0	65658-4	0
2	27,386	98.4949	351.9136	927	90.0551	270.0756	14.37488
ENVISAT11_45							
1	27386U	02009A	11313.04	1.29E−06	00000–0	57693-4	0
2	27,386	98.4914	19.4823	1010	103.3597	256.7693	14.37489
ENVISAT11_49							
1	27386U	02009A	11341.44	3.12E−06	00000–0	11894-3	0
2	27,386	98.488	47.5222	1075	91.0838	269.0472	14.37494
ENVISAT12_01							
1	27386U	02009A	12004.08	1.78E−06	00000–0	74114-4	0
2	27,386	98.4832	74.794	989	85.8951	274.2355	14.37491
ENVISAT12_05							
1	27386U	02009A	12032.06	1.52E−06	00000–0	65227-4	0
2	27,386	98.4795	102.3966	955	85.7339	274.3955	14.37497
ENVISAT12_09							
1	27386U	02009A	12060.04	−9.1E−06	00000–0	−28,802	0
2	27,386	98.4726	129.9827	1075	89.2564	270.8757	14.37485
ENVISAT12_13							
1	27386U	02009A	12088.09	8.5E−07	00000–0	42901-4	0
2	27,386	98.4794	157.6584	1138	92.0005	268.1318	14.37493

References

1. Fussen, D., Dekemper, E., Errera, Q., Franssens, G., Mateshvili, N., Pieroux, D., Vanhellemont, F.: The ALTIUS mission. Atmospheric Measurement Techniques Discussions (2016). https://doi.org/10.5194/amt-2016-213

2. Bermyn, J., Du Pre, T., Bernaerts, D., Baudoux, D.: Proba 'spacecraft family' small autonomous satellites-a Belgian innovative exportproduct. In: Proceedings of the 4S Symposium: Small Satellites, Systems and Services, ESA SP-571 (2004)

3. Fussen, D., Vanhellemont, F., Dodion, J., Bingen, C., Mateshvili, N., Daerden, F., Fonteyn, D., Errera, Q., Chabrillat, S., Kyrölä, E., Tamminen, J., Sofieva, V., Hauchecorne, A., Dalaudier, F.,

Bertaux, J.-L., Renard, J.-B., Fraisse, R., d'Andon, O.F., Barrot, G., Guirlet, M., Mangin, A., Fehr, T., Snoeij, P., Saavedra, L.: A global OClO stratospheric layer discovered in GOMOS stellar occultation measurements. Geophys. Res. Lett. **33**, L13815 (2006). https://doi.org/10.1029/2006GL026406

4. Jones, A., Urban, J., Murtagh, D.P., Eriksson, P., Brohede, S., Haley, C., Degenstein, D., Bourassa, A., von Savigny, C., Son-kaew, T., et al.: Evolution of stratospheric ozone and water vapour time series studied with satellite measurements. Atmos. Chem. Phys. **9**, 6055–6075 (2009)

5. Montzka, S.A., Dutton, G.S., Yu, P., Ray, E., Portmann, R.W., Daniel, J.S., Kuijpers, L., Hall, B.D., Mondeel, D., Siso, C., et al.: An unexpected and persistent increase in global emissions of ozone-depleting CFC-11. Nature. **557**, 413 (2018)

6. Hoots, F.R., Roehrich, R.L.: Spacetrack Report #3: Models for Propagation of the NORAD Element Sets. U.S. Air Force Aerospace Defense Command, Colorado Springs, CO. (1980)

7. Bennett, J., Sang, J., Smith, C., Zhang, K.: Improving low-Earth orbit predictions using two-line element data with bias correction. In: Advanced Maui Optical and Space Surveillance Technologies Conference. vol. 1, p. 46 (2012)

8. Flohrer, T., Krag, H., Klinkrad, H.: Assessment and categorization of TLE orbit errors for the US SSN catalogue. Risk. 8, 10–11 (2008)

9. Levit, C., Marshall, W.: Improved orbit predictions using two-line elements. Adv. Space Res. **47**, 1107–1115 (2011)

10. Aida, S., Kirschner, M., Wermuth, M., Kiehling, R.: Collision avoidance operations for LEO satellites controlled by GSOC. Space OpsAIAA. **71**, 2010–2298 (2010)

11. Fortescue, P., Swinerd, G., Stark, J.: Spacecraft systems engineering. Wiley, Hoboken (2011)

12. Hoots, F.R.: Reformulation of the Brouwer geopotential theory for improved computational efficiency. Celest. Mech. **24**, 367–375 (1981)

13. Benveniste, J., Roca, M., Levrini, G., Vincent, P., Baker, S., Zanife, O., Zelli, C., Bombaci, O.: The radar altimetry mission: RA-2, MWR, DORIS and LRR. ESA Bull. **106**, 25101–25108 (2001)

14. Kuiper, D., Garcia Matatoros, M.: Analysis of Envisat orbit maintenance strategies to improve/increase Envisat ASAR interferometry opportunities. In: Proceedings of the 20th International Symposium on Space Flight Dynamics, Annapolis, Maryland, USA, 24–28 September (2007)